Journal of Wind Engineering & Industrial Aerodynamics 229 (2022) 105139

Contents lists available at ScienceDirect

Journal of Wind Engineering & Industrial Aerodynamics

journal homepage: www.elsevier.com/locate/jweia

High-blockage corrections for circular arcs at transitional Reynolds numbers

Jean-Baptiste R.G. Souppez [a,b], Ignazio Maria Viola [a,*]

[a] School of Engineering, Institute for Energy Systems, University of Edinburgh, Edinburgh, EH9 3DW, United Kingdom
[b] Mechanical, Biomedical and Design Engineering Department, School of Engineering and Technology, College of Engineering and Physical Sciences, Aston University, Birmingham, B4 7ET, United Kingdom

ARTICLE INFO

Keywords:
Blockage correction
Aerofoil
Hydrofoil
Cambered plate
Water tunnel
Towing tank

ABSTRACT

Model-scale testing might suffer from blockage effects due to the finite dimensions of the test section. Measurements must be corrected to predict the forces that would have been measured in unconfined conditions. Blockage corrections are well-established for streamlined and bluff bodies, while more data is needed to develop corrections for bodies that generate both high lift and large wakes. In this work, towing tank and water tunnel tests of two-dimensional circular arcs are employed to develop a correction for a blockage ratio, i.e. the ratio of the frontal area of the geometry to the cross-sectional area of the test section, up to 0.2477. Experiments are conducted at positive incidences between the ideal angle of attack and deep-stall at transitional Reynolds numbers from 53 530 to 218 000. The results show that a linear blockage correction can be devised for the whole range of tested blockage ratios. Furthermore, the critical angle of attack and Reynolds number at which the force crisis occurs is independent of the blockage ratio. These results may allow extending the range of model sizes that can be tested in water and wind tunnels and may contribute to the accurate accounting of blockage effects at transitional Reynolds number conditions.

1. Introduction

Model testing undertaken in experimental facilities, such as towing tanks, water and wind tunnels, suffers from blockage effects. This is caused by the physical restrictions of the test section compared to the model size. The restricted cross-sectional area leads to an increase in flow speed around the tested geometry compared to an unblocked (or free) flow, yielding higher forces. Consequently, blockage correction is needed to estimate unconstrained force coefficients.

Glauert (1933) proposed a blockage correction for streamlined bodies. Further guidance on wind tunnel experiments and blockage corrections were introduced by Pankhurst and Holder (1952) and later Pope and Harper (1966), more recently updated by Barlow et al. (1999). These were however shown to yield poor agreement with experimental data for largely separated flows (Jeong et al., 2018; Arredondo-Galeana, 2019).

Bluff bodies, such as flat plates normal to the flow, have also been investigated. Allen and Vincenti (1944) provided a blockage correction, later shown to be only valid for low blockage ratios by Dalton (1971). Maskell (1963) proposed a blockage correction applicable to high blockage ratios. The assumptions underpinning Maskell's work were first refined by Cowdrey (1968), then Toebes (1971) and later Alexander (1978), before a revised blockage correction was proposed by Hackett and Cooper (2001) following extensive testing. Blocked flow normal to a flat plate has also been investigated to tackle separated flow aerodynamics (Lasher, 2001) who concluded on the need for further work to be conducted on other geometries experiencing separated flow.

The Engineering Science Data Unit (ESDU) summarises the corrections for bluff bodies in the ESDU 80024 guidelines (ESDU, 1998). These include cylinders in subcritical and transcritical regimes, the latter treated as a quasi-streamlined body.

Guidance on the maximum recommended solid-body blockage ratio for low-speed wind tunnels has been provided by Pope and Harper (1966). The same guidelines can be equally adopted irrespective of the working fluid such as, for instance, water tunnels. Their recommendation of 0.10 was then revised to 0.075 by Barlow et al. (1999). More recently, values of 0.050 or lower have been suggested (Lasher et al., 2005; Prasanth et al., 2006; Ross and Altman, 2011; Malizia and Blocken, 2020). However, with the increased use of flow diagnostics techniques, such as particle image velocimetry (PIV), higher blockage ratios than the previously cited guidelines are often employed to increase the spatial resolution (Miklasz et al., 2010; Kellnerová et al., 2012; Marchand et al., 2017; Molina et al., 2019; Bot, 2020). Insight into the ability to correct force measurements at blockage ratios higher than the current guidelines would therefore be valuable.

* Corresponding author.
E-mail address: i.m.viola@ed.ac.uk (I.M. Viola).

https://doi.org/10.1016/j.jweia.2022.105139
Received 5 April 2022; Received in revised form 15 August 2022; Accepted 15 August 2022
Available online 5 September 2022

Table 1
Geometric dimensions of the three circular arcs.

Circular Arc	Small	Medium	Large
Chord, c (mm)	100	150	200
Span, s (mm)	370	370	370
Camber, y_c (mm)	22.32	33.48	44.64
Thickness, t (mm)	1.80	1.80	1.80

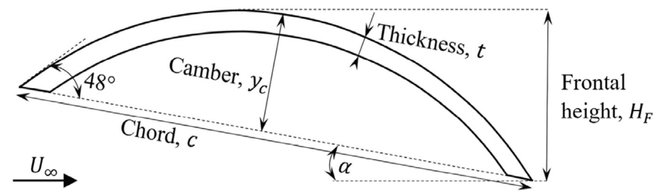

Fig. 1. Definition of the geometric parameters.

Blockage effects can modify the critical Reynolds number of circular cylinders (Coutanceau and Bouard, 1977), which is the minimum Reynolds number (Re) at which laminar-to-turbulent transition occurs upstream of the separation point (Schewe, 2001). Therefore, tests undertaken in the presence of a high blockage effect might result in substantially different flow fields than tests at the same Re but in unconstrained conditions. Thin foils are also subject to a force crisis (Schmitz, 1942; Tank et al., 2021). On some foils such as circular arcs, however, this is because of a different underlying mechanism than for cylinders. The sharp leading edge triggers laminar-to-turbulent transition even at low Re and the flow relaminarise near the reattachment point (Souppez et al., 2022). The drag crisis occurs when relaminarisation is suppressed. Circular arcs have been studied at transitional Re for applications such as compressor blades (Lieblein, 1960), micro aerial vehicle wings (Hein and Chopra, 2007), Savonius turbines (Damak et al., 2018) and model-scale yacht sails (Cyr and Newman, 1996; Collie et al., 2004; Lasher and Sonnenmeier, 2008). However, it is yet to be determined whether a high blockage ratio affects the critical Reynolds number at which relaminarisation is suppressed.

In this paper, a two-dimensional (2D) highly-cambered circular arc with a sharp leading edge, i.e. a cambered thin plate with uniform curvature, is considered. The aim of this paper is to investigate how the force measurements of such geometry can be corrected for high blockage ratios. The effect of blockage on the forces and the laminar or turbulent state of the boundary layer is investigated for a wide range of blockage ratios exceeding conventional recommendations. Furthermore, the impact of free surface deformation on force measurements is discussed.

The remainder of the paper is structured as follows. The geometry, the test facilities and the uncertainty analysis are described in Section 2. The results, including the validation of the force measurements against published data and the blockage correction devised for the lift-generating body under consideration are presented in Section 3. Finally, the main conclusions from this study are summarised in Section 4.

2. Methodology

2.1. Geometry

To span across a wide range of chord-based Reynolds number conditions ($53\,530 < Re < 218\,000$), three highly-cambered, thin, circular arcs with a sharp leading edge were manufactured. The main geometric characteristics are presented in Fig. 1 and Table 1. The camber-to-chord ratio for all arcs is identical to that tested by Velychko (2014) and Bot (2020), namely $y_c/c = 0.2232$. The thickness-to-chord ratio t/c ranges between 0.0090 and 0.0180, i.e. smaller than half that employed by Velychko (2014) and Bot (2020), where $0.0357 < t/c < 0.0400$. This is made possible by manufacturing the arcs from carbon fibre prepreg. Wet and dry sandpaper up to 2500 grit was employed to achieve a hydrodynamically smooth surface. This exceeds the 300–400 grit wet and dry sandpaper finish required in the ITTC (2017) experimental guidelines Based on the ISO6344-1:1998 (ISO, 1998), the median grain size for 2500 grit sandpaper is 8.4 ± 0.5 μm, while it would be 35.0 ± 1.5 μm for 400 grit. In comparison, the required grain size to artificially trigger transition is 500 μm (ITTC, 2017).

For this geometry and Reynolds number range, Souppez et al. (2022) showed that the ideal angle of attack α is 11°. This is the angle at which the stagnation point is at the leading edge. At angles of attack lower than 11°, the trend of the forces with α is dominated by changes in the recirculation flow on the pressure side of the arc (Bot, 2020). At $\alpha \geq 23°$, the flow separates at the leading edge and does not reattach (Souppez et al., 2021). Therefore experiments were undertaken at $10° < \alpha < 20°$ in both the towing tank and the water tunnel.

Lift and drag coefficients, C_L and C_D, were computed as

$$C_L = \frac{L}{\frac{1}{2}\rho c s U_\infty^2}, \tag{1}$$

$$C_D = \frac{D}{\frac{1}{2}\rho c s U_\infty^2}, \tag{2}$$

where L is the measured lift, D is the measured drag, $\rho = 998.33\,\mathrm{kg\,m^{-3}}$ is the density of the water taken as that of fresh water at a temperature of 19.4 °C (ITTC, 2011), c is the chord, s is the span and U_∞ is the velocity of the carriage in the towing tank and the freestream velocity in the water tunnel.

The blockage ratio is defined as the ratio of the frontal area of the model divided by the area of the test section. As the present model is extruded across the side walls of the test section, the blockage ratio is the ratio of the frontal height H_F of the model to the distance between the side walls d. Within the range of tested angles of attack, the frontal height of the model is

$$H_F = r - (r - y_c)\cos\alpha + \frac{c}{2}\sin\alpha, \tag{3}$$

where the radius of curvature is

$$r = \frac{y_c}{2} + \frac{c^2}{8y_c}. \tag{4}$$

The arc length is

$$l = \arccos\left(1 - \frac{c^2}{2r^2}\right) r. \tag{5}$$

2.2. Towing tank

Force measurements for all three arcs were undertaken in Solent University's towing tank, which is 60 m long, 3.7 m wide and 1.8 m deep (Dewavrin and Souppez, 2018). Each arc was fitted between end plates 340 mm long and 340 mm wide to achieve an effective infinite aspect ratio. The top end plate was located 100 mm below the free surface, and the spanwise axis of the circular arc was vertical and located in the middle of the tank's side walls. The experimental setup is depicted in Fig. 2.

The small arc ($c = 100$ mm) was tested at $Re = 53\,530$ (as in Velychko 2014), and $Re = 68\,200$ (as in Bot 2020). The large arc ($c = 200$ mm) was tested at $Re = 218\,000$ (as in Bot 2020). To provide intermediate data, the medium arc ($c = 150$ mm) was tested at $Re = 150\,000$.

The blockage ratio was varied by means of adjustable sidewalls 1200 mm long and 1200 mm wide. They extended $3c$ upstream and $2c$ downstream of the circular arc, and were separated by a transverse distance d, shown in Fig. 3. The towing tank experimental setup is pictured in Fig. 4. A total of four distances were investigated in this study,

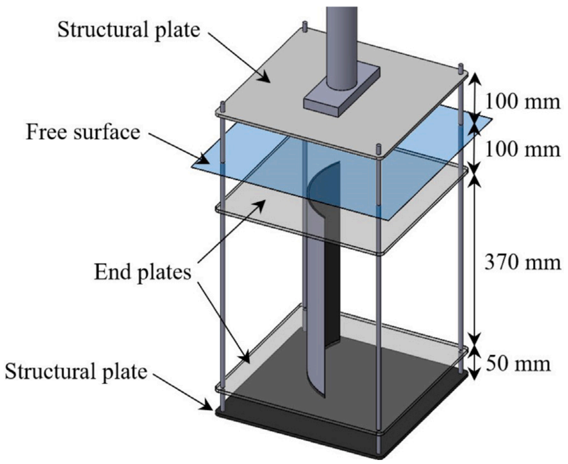

Fig. 2. Schematic drawing of the model and of the supporting rig adopted in the towing tank.

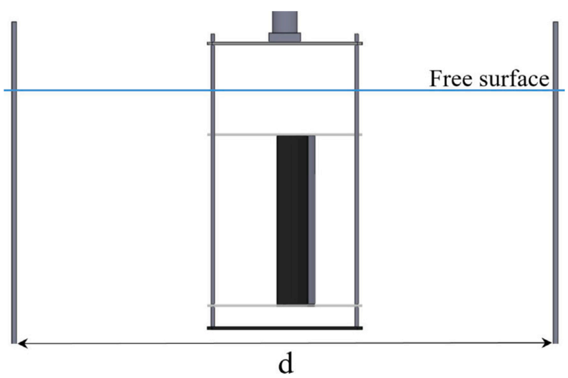

Fig. 3. End elevation of the model, supporting rig and side walls employed in the towing tank.

namely $d = 3700$ mm, 1180 mm, 550 mm and 340 mm. The 3700 mm width is the full towing tank width, and thus the side walls were not utilised. The intermediate values $d = 1180$ mm and 550 mm were driven by the practical ability to fix the side walls to the carriage. The distance $d = 340$ mm corresponds to the water tunnel height, therefore yielding an identical blockage ratio.

The experimental rig was fitted to a single-post dynamometer equipped with potentiometers, which have an accuracy of ± 0.001 N. The data acquisition was automatically triggered after the desired test speed was reached. The lift and drag were sampled at 1000 Hz for a minimum of 6 s. The forces created by the test rig, including end plates, were first measured without the circular arc at the various test speeds. These were later subtracted from the time-averaged total force measurements to yield the lift and drag on the circular arc alone.

2.3. Water tunnel

Additional force measurements were conducted on the large (c = 200 mm) arc at $Re = 68\,200$ in the open water tunnel with a free surface at the University of Edinburgh. This water tunnel is 8 m long and 0.4 m wide, and the water height was set at 0.34 m, resulting in a Froude number of 0.19. The arc was vertically centred on the water column, with the suction side towards the free surface. No end plates were fitted as the model spanned across the water tunnel's width, with the exception of small gaps either side to avoid contact. The experimental setup is presented in Fig. 5.

The data was sampled at 100 Hz for 45 s, using the six-axis force/torque sensor Nano 17 IP68 from ATI Inc., with a resolution of

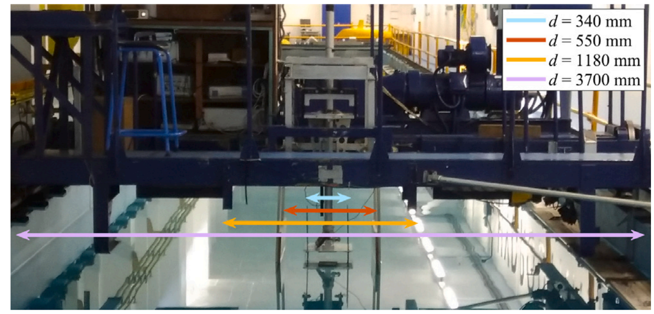

Fig. 4. Picture of the experimental towing tank setup for $d = 550$ mm. The other tested positions of the sidewalls are indicated by coloured arrows. (For interpretation of the references to colour in this figure legend, the reader is referred to the web version of this article.)

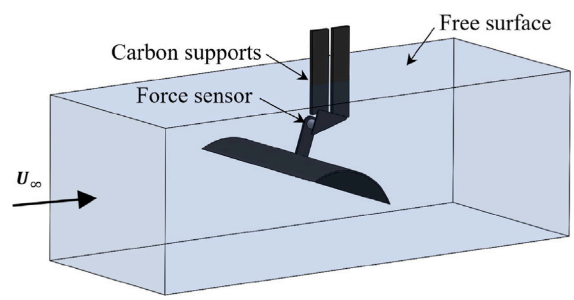

Fig. 5. Schematic drawing of the model and of the supporting rig adopted in the water tunnel.

$\pm 160^{-1}$ N. The spanwise flow is uniform within $\pm 0.00568\ U_\infty$ in the central 350 mm of the water tunnel, and unaffected by the bottom boundary layer at the depths where measurements were made (Arredondo-Galeana, 2019). Tests were performed both with the free surface allowed to deform, and with a solid top plate enclosing the water tunnel.

As for the towing tank tests, force measurements in the water tunnel were undertaken both with and without the arc attached to the test rig. The difference between the two time-averaged force measurements yielded the lift and drag forces. The lift and drag coefficients were then computed using Eqs. (1) and (2).

2.4. Uncertainty analysis

The uncertainty due to fixed errors that do not vary during the measurements is computed from the estimate of the total bias limit. Following the nomenclature of the ITTC (2014), the total bias limit of the force coefficient $B_T(C_F)$, where C_F is either C_L or C_D, is

$$B_T(C_F) = \left[\left(\frac{\partial C_F}{\partial \rho} B(\rho) \right)^2 + \left(\frac{\partial C_F}{\partial A} B(A) \right)^2 + \left(\frac{\partial C_F}{\partial U_\infty} B(U_\infty) \right)^2 + \left(\frac{\partial C_F}{\partial F} B(F) \right)^2 \right]^{\frac{1}{2}}, \quad (6)$$

where $B(\rho)$, $B(A)$, $B(U_\infty)$ and $B(F)$ are the bias limits of the density, the area, the freestream velocity and the force, respectively. Expanding the derivatives of the sensitivity coefficients in Eq. (6) yields

$$B_T(C_F) = \left[\left(\frac{-2F}{\rho^2 U_\infty^2 A} B(\rho) \right)^2 + \left(\frac{-2F}{\rho U_\infty^2 A^2} B(A) \right)^2 + \left(\frac{-4F}{\rho U_\infty^3 A} B(U_\infty) \right)^2 + \left(\frac{2}{\rho U_\infty^2 A} B(F) \right)^2 \right]^{\frac{1}{2}}. \quad (7)$$

Table 2
Summary of the bias limits in the two experimental facilities.

Magnitude of bias limits	Towing tank	Water tunnel
$B(\rho)$ (kg m^{-3})	0.03968	0.01387
$B(A)$ (m^2)	0.00000025	0.00000025
$B(U_\infty)$ (m s^{-1})	0.005	0.00568
$B(F)$ (N)	0.0005	0.0065
$B(\alpha)$ (deg)	0.025	0.025
$B_{max}(C_L)$	0.01296	0.01651
$B_{max}(C_D)$	0.00966	0.01018

where $A = cs$. The bias limits $B(\rho)$, $B(A)$, $B(U_\infty)$ and $B(F)$ for the towing tank (TT) and the water tunnel (WT) are estimated as follows.

The water temperature T was recorded at the start and end of each day in the towing tank. The temperature ranged between 19.2 °C and 19.6 °C. The median temperature was T_{TT} = 19.4 °C ±0.2 °C and the bias limit is $B(T_{TT}) = 0.2$ °C. In the water tunnel, the temperature was sampled continuously at 0.0167 Hz. The median temperature was $T_{WT} = 21.6510$ °C, with a minimum of 21.5885 °C and a maximum of 21.7135 °C. The bias limit is $B(T_{WT}) = 0.0625$ °C. Following the ITTC (2011) guidelines, the bias limit of the water density is

$$B(\rho) = \left|\frac{\partial \rho}{\partial T}\right| B(T), \tag{8}$$

where the sensitivity coefficient is

$$\left|\frac{\partial \rho}{\partial T}\right| = \left|0.0552 - 0.0154T + 0.000120T^2\right|. \tag{9}$$

Eqs. (8) and (9) give $B(\rho_{TT}) = 0.039\,68$ kg m^{-3} for the towing tank, and $B(\rho_{WT}) = 0.013\,87$ kg m^{-3} for the water tunnel.

The bias limits for the chord and span are taken as half the smallest measuring division, namely ±0.5 mm. Consequently, the bias limit of the area is identical for both facilities, and $B(A_{TT}) = B(A_{WT}) = 0.000\,000\,25$ m^2.

In the towing tank, the freestream velocity bias limit $B(U_{\infty,\,TT})$ is taken as half the smallest recording division, namely 0.005 m s^{-1}. Conversely, in the water tunnel, laser Doppler velocimetry measurements by Arredondo-Galeana (2019) have shown that $B(U_{\infty,\,WT}) = 0.005\,68$ m s^{-1}.

For the force measurements, the bias limits are given by the manufacturer's specifications of the force sensors. The bias limits are $B(F_{TT}) = 0.0005$ N in the towing tank and $B(F_{WT}) = 0.006\,25$ N in the water tunnel.

The angle of attack was measured with a digital inclinometer. The arc is placed in no-flow condition and the position is adjusted until the intended incidence is achieved within the instrument's accuracy of ±0.025°. The angle of incidence is further checked once the desired flow speed is reached to ensure that the model did not rotate. The bias limit is $B(\alpha) = 0.025°$. Note that the uncertainty inherent to the angle of attack is not considered in the computation of the bias limit of the lift and drag coefficients (Eq. (7)).

The magnitude of the bias limits are summarised in Table 2. The table also includes the maximum bias limits of the lift ($B_{max}(C_L)$) and drag ($B_{max}(C_D)$) coefficients, computed with Eq. (7) using the minimum values of the area (smallest arc) and freestream velocity (lowest Re) in the towing tank, and the minimum recorded lift and drag in each facility.

The random error associated with each measurement is the precision, P. This is estimated at the 95% confidence level (i.e. two standard deviations, 2σ) of the sampled instantaneous force measurements for each individual test, so that

$$P = \frac{2\sigma}{\sqrt{n}}, \tag{10}$$

where $n = 1$ because no repeats were undertaken.

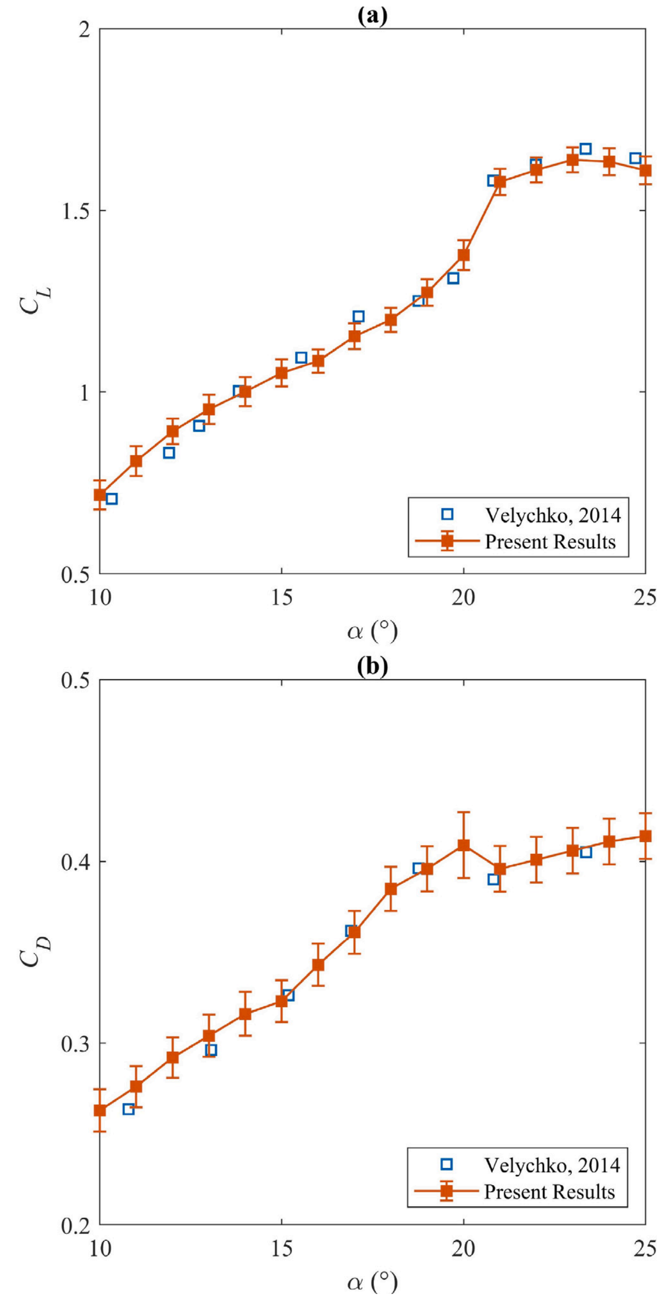

Fig. 6. Lift (a) and drag (b) coefficients versus the angle of attack for the small arc tested in the towing tank with d = 3700 mm and comparison with the wind tunnel tests by Velychko (2014) on an arc with $t/c = 0.0357$ and $AR = 10$ spanning across the wind tunnel height. Both arcs are tested at $Re = 53\,530$ and no blockage correction is applied.

The uncertainty is estimated by combining the bias limit and the precision as follows

$$U = \sqrt{B^2 + P^2}. \tag{11}$$

The uncertainty for both the lift and the drag coefficients is shown by vertical error bars in Fig. 6, but these are omitted in subsequent figures for clarity. Furthermore, given that the uncertainty on the angle of attack is small ($B(\alpha) = 0.025°$) compared to the smallest sample interval of one degree, horizontal error bars for the angle of attack are not shown.

2.5. Established blockage corrections

This section summarises the blockage corrections of ESDU 76028 (ESDU, 1995) for 2D subsonic flow in closed wind-tunnels and ESDU 80024 (ESDU, 1998) for bluff bodies in confined flows. Both corrections are compared in Section 3.4 with the correction developed in this work.

The blockage ratio is defined as the ratio of the frontal area of the geometry, $A_F = H_F s$, to the area of a tunnel cross-section $A_S = sd$. For two-dimensional sections spanning the whole tunnel, this can also be expressed as the ratio of the frontal height of the model over the height of the test section, H_F/d. Note that H_F/d increases monotonically with α in this work (Eq. (3)).

The ESDU 76028 blockage correction (ESDU, 1995) predicts a reduction in the aerodynamic coefficients proportional to due to a change in the dynamic pressure, and a change in the angle of attack due to changes in the streamline curvature.

The ratio between the corrected force coefficient C_F (with C_F being, for example, C_L or C_D) and the measured blocked force coefficient C_{FB} is

$$\frac{C_F}{C_{FB}} = \left(1 + \epsilon_B\right)^{-1}, \tag{12}$$

where

$$\epsilon_B = \frac{\pi A}{6d^2}\left(1 + 1.2\frac{t}{c}\right)\left(1 + 1.1\frac{c}{t}\alpha^2\right) + \frac{c}{4d}(1 + 0.4)C_{DB}, \tag{13}$$

α is in radians, $A = lt$ is the cross-sectional area of the model and C_{DB} is the measured blocked drag coefficient.

The change in the angle of attack is

$$\Delta\alpha = \frac{\pi}{24}\left(\frac{c}{d}\right)^2\left(\frac{C_{LB}}{4} + C_{MB}\right), \tag{14}$$

where C_{LB} is the blocked lift coefficient; C_{MB} is the blocked moment coefficient at the quarter chord, positive nose up. Because C_{MB} was not measured in the present work, we consider two limiting conditions: $C_{MB} = 0$, which is valid in potential flow, and $C_{MB} = C_{NB}\, c/4$, which is the moment at the quarter chord due to a chordnormal force (whose coefficient is $C_{NB} = C_{LB}\cos\alpha + C_{DB}\sin\alpha$) through the mid chord.

The ESDU 80024 blockage correction (ESDU, 1998) distinguishes between bluff-body flow and quasi-streamlined flow, depending on whether flow separation occurs upstream or downstream of the maximum streamnormal thickness of the body. For the circular arc under consideration, flow visualisation by Bot (2020) and Souppez et al. (2022) have shown that trailing-edge separation occurs downstream of the maximum streamnormal thickness of the body in both subcritical and supercritical conditions. The correction for quasi-streamlined flow is therefore applied.

It is noted that, in the absence of information regarding where separation occurs, an alternative selection criterion is provided to select the most appropriate blockage correction method. For $C_D < 0.8$ and $Re > 4 \times 10^4$, the quasi-streamlined approach is recommended (ESDU, 1998). For the flow conditions considered in the present work, $C_D < 0.5$ and $Re = 6.82 \times 10^4$, this further confirms that the correction for quasi-streamlined flow is the most appropriate.

Based on ESDU 80024, the ratio between the corrected and the blocked force coefficients is

$$\frac{C_F}{C_{FB}} = 1 - \lambda_1\lambda_5\left(1 + \lambda_2\frac{c}{y_c}\right)\left(\frac{H_F}{d}\right)^2 - \frac{C_{DB}}{2}\frac{H_F}{d}, \tag{15}$$

where $\lambda_1 = 0.823$ is the tunnel shape factor for a rectangular cross-section; $\lambda_2 = 1$ is the body shape factor, whose unit value is recommended for elliptical cylinders. It is noted, however, that the effect of different choices of λ_2 is marginal on the overall correction. Finally, or for lift-generating bodies,

$$\lambda_5 = 1 + 1.1\frac{c}{y_c}\alpha^2, \tag{16}$$

with α in radians.

3. Results

3.1. Validation of the experimental setup

Towing tank tests at $Re = 53\,530$ are compared with the wind tunnel tests of Velychko (2014) for the lift and drag in Fig. 6a and Fig. 6b, respectively. Both tests were undertaken at the same Re and on a circular arc with the same camber-to-chord ratio ($y_c/c = 0.2232$). The differences are in the higher thickness-to-chord ratio ($t/c = 0.0357$) and the higher physical aspect ratio (AR) of Velychko's arc ($AR = 10$). However, in both tests, the arcs had an infinite effective aspect ratio because the arc in the towing tank was equipped with end plates, and that in the wind tunnel spanned the whole tunnel (the top and bottom walls acted as end plates).

The agreement between the force coefficients of the two tests suggests that the end plates used in the towing tank are effective in reproducing an arc with an infinite aspect ratio. Furthermore, because the thickness-to-chord ratios of 0.0357 (Velychko, 2014) and 0.0180 provide similar results, the thickness effect is considered negligible. Consequently, the results can be generalised to infinitely thin arcs. This is particularly relevant to the model testing of membranes and sails, which have a thickness-to-chord ratio at least one order of magnitude lower than the circular arcs considered in this study.

3.2. Uncorrected force measurements

The results for the uncorrected, blocked force measurements are depicted in Figs. 7a and 7b for the lift and drag, respectively (the subscript B for 'blocked' is omitted in this section for brevity). These include all tested Re in the towing tank, as well as $Re = 68\,200$ in the water tunnel. The latter experiment was realised both with a top plate (TP) and without one, allowing free surface (FS) deformation. There is a noticeable offset at $Re = 68\,200$ between the values achieved in the towing tank and those of the water tunnel due to blockage. Blockage effects are negligible in the towing tank experiments without sidewalls because of the low blockage ratios, $0.0030 < A_F/A_S < 0.0047$, which do not warrant for blockage correction (Barlow et al., 1999). Conversely, blockage effects are significant in the water tunnel where $0.1461 < A_F/A_S < 0.2477$.

For this geometry and flow condition range, the force trends with the angle of attack have been discussed in details by Souppez et al. (2022) and Bot (2020), and it is here summarised. At $Re = 218\,000$, C_L increases up to $\alpha \approx 8$, where the lift curve begins to decrease due to the trailing-edge separation point moving upstream with α. This effect is substantial only up to the ideal angle of attack ($\alpha \approx 11$), where the stagnation moves to the concave side of the arc and C_L increases again with α. At these high angles of attack, the flow separates at the leading edge forming a turbulent leading-edge separation bubble, and a turbulent boundary layer exists between the reattachment point and the trailing-edge separation point.

In contrast, at lower Re, the boundary layer is laminar for low α, and thus the trailing-edge separation point is closer to the leading edge and the lift is lower than for higher Re at the same α. At $Re = 53\,530$, the boundary layer turns into turbulent when the leading-edge separation bubble is formed, and thus C_L collapses to that at higher Re at $\alpha \approx 11°$. At $Re = 150\,000$ and $68\,200$, the flow turns into turbulent within the leading-edge separation bubble but relaminarisation occurs near the reattachment point, leading to a laminar boundary layer. At $Re = 150\,000$ and $68\,200$, turbulent trailing-edge separation occurs only for angles of attack greater than $\alpha \approx 14°$ and $20°$, respectively.

At the angle of attack where trailing-edge separation turns from laminar to turbulent, the lift and drag show a step increase and decrease, respectively, known as the force crisis (Bot et al., 2016). It occurs for a combination of critical angles of attack and critical Reynolds numbers (Souppez et al., 2022) such as, for example, $20° < \alpha < 21°$ for $Re = 53\,530$. A key finding is revealed in Fig. 7 by the three

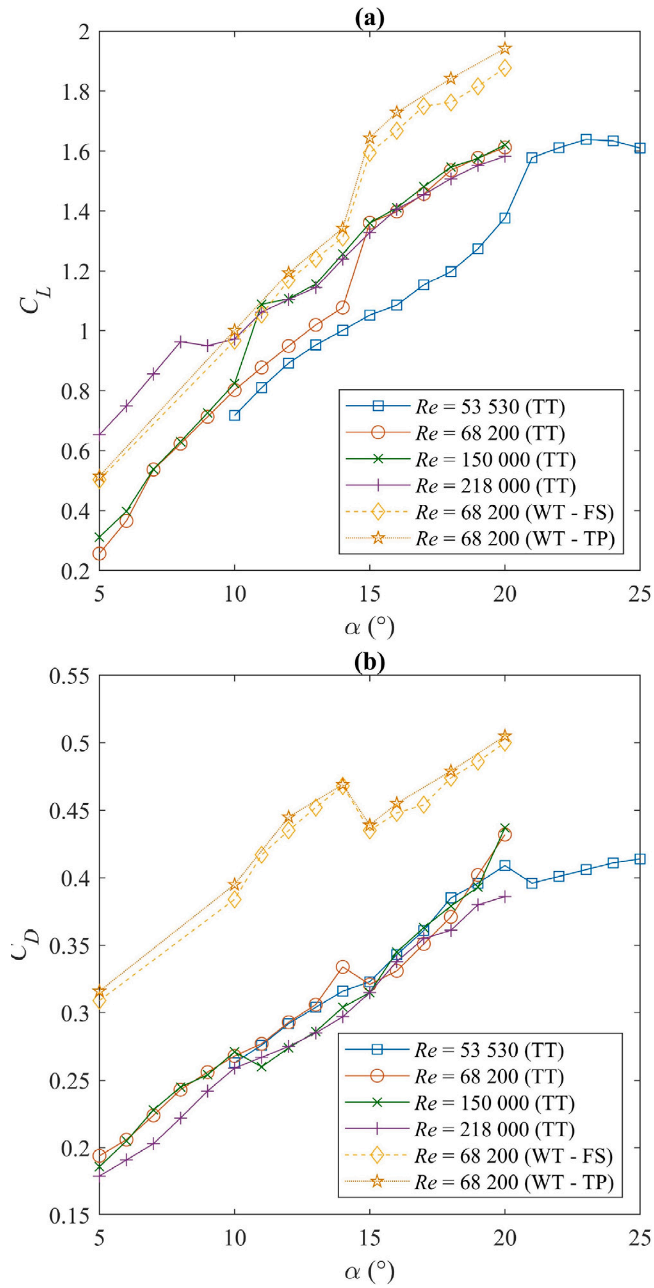

Fig. 7. Lift (a) and drag (b) coefficients versus the angle of attack recorded in the towing tank (TT) and water tunnel (WT), with both a top plate (TP) and free surface (FS) able to deform.

curves at $Re = 68\,200$ with two different blockage values: the blockage ratio does not alter the critical angle of attack within the 1° accuracy associated with the incidence increment employed in this study. The occurrence of turbulent trailing-edge separation is therefore unaffected by the blockage ratio. This justifies using a smooth and linear blockage correction that does not predict non-linear variations associated with changes in the boundary layer state. In fact, the following subsection shows that a linear correction allows a good fit of the experimental data.

3.3. Blockage correction

The methodology for the development of an experimental blockage correction for lift-generating bodies with large trailing-edge separation is presented in this section. The correction is devised solely using the towing tank data, while the water tunnel measurements are used to assess the accuracy of the extrapolation of the forces for unblocked conditions. The ratio between the corrected and the uncorrected force coefficients (C_L/C_{LB} and C_D/C_{DB} for lift and drag, respectively) are depicted in Fig. 8 for different blockage ratios and $Re = 68\,200$ (a–b), $Re = 150\,000$ (c–d) and $Re = 218\,000$ (e–f). It is noted that, despite the high blockage ratios ($A_F/A_S > 0.15$), the ratios between the corrected and the uncorrected force coefficients remain linear with the blockage ratio.

The error bars in Fig. 8 show that the linear trends are within the uncertainty of the experimental results. A higher uncertainty is observed at $Re = 68\,200$ compared to $Re = 150\,000$ and $Re = 218\,000$, due to the lower magnitude of the forces measured. Additionally, the uncertainty at $\alpha = 10°$ is greater than that at $\alpha = 15°$ and $\alpha = 20°$. This is understood as the effect of the pressure side recirculation bubble, evidenced by Bot (2020). In fact, for incidences well below the ideal angle of attack, a large recirculation bubble occurs, not yielding a linear blockage correction (Souppez and Viola, 2022). While a large recirculation bubble is not be expected on the pressure side at $\alpha = 10°$ (Bot, 2020), the ideal angle of attack at $Re = 68\,200$ has been shown to be $\alpha = 11°$ (Souppez and Viola, 2022). Recirculation on the pressure side is therefore assumed to be the origin of the higher uncertainty $\alpha = 10°$ compared to $\alpha = 15°$ and $\alpha = 20°$.

For every Reynolds number and angle of attack, C_L/C_{LB} and C_D/C_{DB} are fitted with linear regressions $y = a_L x + b_L$ and $y = a_D x + b_D$, respectively. As A_F/A_S vanishes, the ratios C_L/C_{LB} and C_D/C_{DB} tend towards unity and thus $b_L = b_D = 1$. The slopes a_L and a_D are presented in Tables 3 and 4. For the intermediate angles of attack, the slope is computed by linear interpolation of the measured values. The corrected lift and drag coefficients are computed using Eq. (17) and Eq. (18), respectively.

$$\frac{C_L}{C_{LB}} = \left(a_L \frac{A_F}{A_S} + 1\right) \tag{17}$$

$$\frac{C_D}{C_{DB}} = \left(a_D \frac{A_F}{A_S} + 1\right) \tag{18}$$

Within this work it is not possible to draw statistically significant conclusions on the effect of blockage on the amplitude of the force fluctuations. In fact, the magnitude of the standard deviation (σ) of C_L and C_D is of the order of 10^{-2}, which is smaller than the experimental uncertainty of the results. This is computed from the instantaneous force measurements sampled at 1000 Hz for a minimum of 6 s. Furthermore, no clear trends of σ with the blockage ratio could be observed for both C_L and C_D.

Table 3
Linear lift correction regression coefficients, a_L.

α	Re = 68 200	Re = 150 000	Re = 218 000
10°	−1.0738	−1.2434	−0.7811
15°	−0.7588	−0.7001	−0.6174
20°	−0.6575	−0.3408	−0.3469

Table 4
Linear drag correction regression coefficients, a_D.

α	Re = 68 200	Re = 150 000	Re = 218 000
10°	−1.8332	−1.4460	−0.8095
15°	−1.4080	−0.3418	−0.4657
20°	−0.6098	−0.2576	−0.2795

3.4. Corrected water tunnel force measurements

First, the proposed blockage correction, which was derived from linear fitting of the towing tank measurements, is here applied to the same set of tests to demonstrate the effect of the linear fit on the

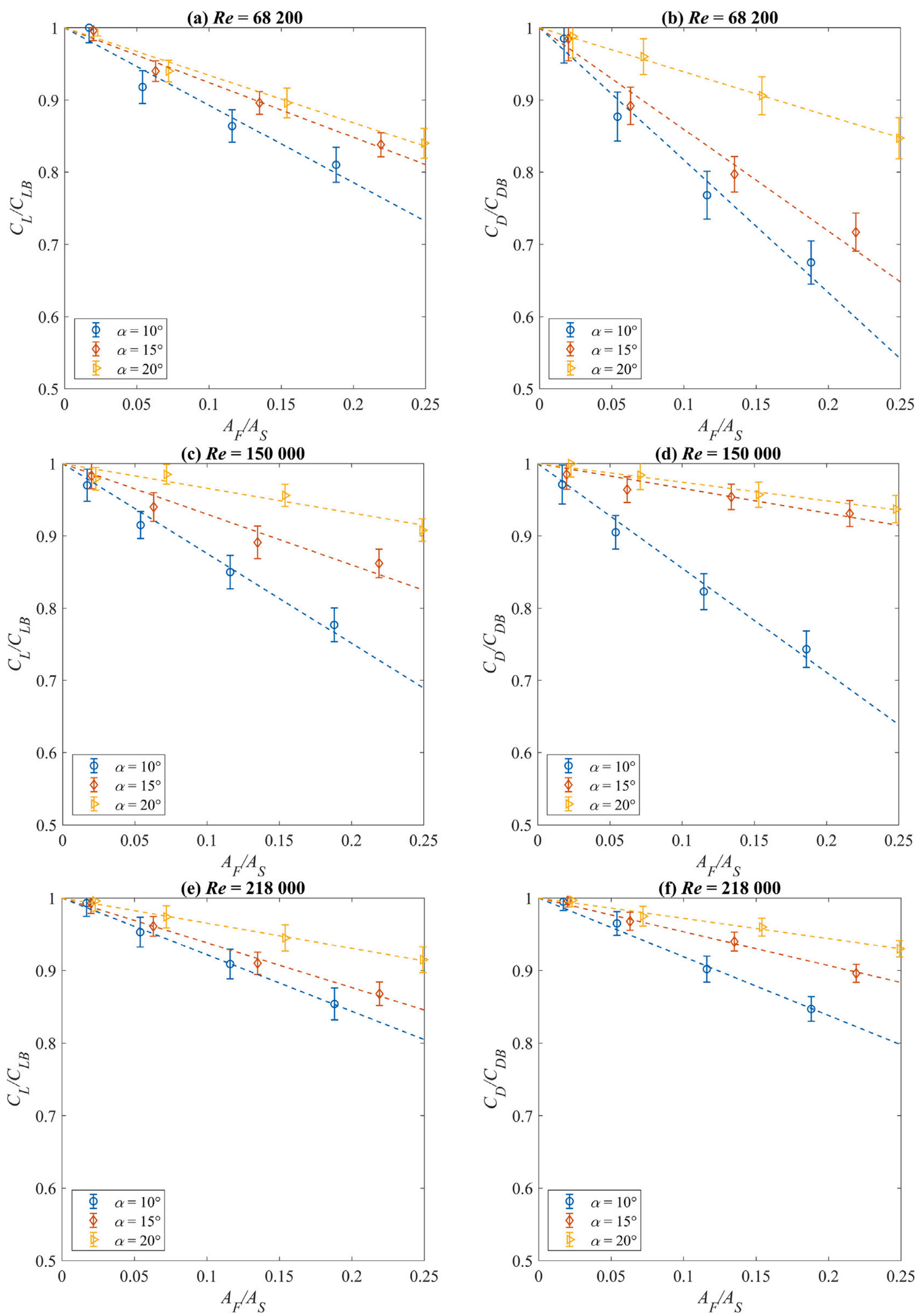

Fig. 8. Ratio of the corrected lift and drag coefficients (C_L, C_D) over their measured values (C_{LB}, C_{DB}) versus the blockage ratio (A_F/A_S) for different angles of attack at Re = 68 200 (a–b), Re = 150 000 (c–d), and Re = 218 000 (e–f). Error bars show the 95% confident interval.

corrected force coefficients. Results are presented in Fig. 9 at Re = 68 200 (a–b), Re = 150 000 (c–d) and Re = 218 000 (e–f). For all tested conditions, the corrected lift and drag collapse to the values measured under nominally unblocked conditions, d = 3700 mm.

We now apply the proposed blockage correction to the water tunnel measurements. The flow conditions in the two sets of experiments have remarkable differences. In the towing tank, the model is constrained by sidewalls for a finite length of 6 chord lengths (sidewalls are 1200 mm long), whilst in the water tunnel the model is confined within a closed duct. Despite these differences, the data measured in the water tunnel collapse onto a single curve once corrected for blockage effects. This is pictured for the lift and drag at Re = 68 200 in Fig. 10a and Fig. 10b,

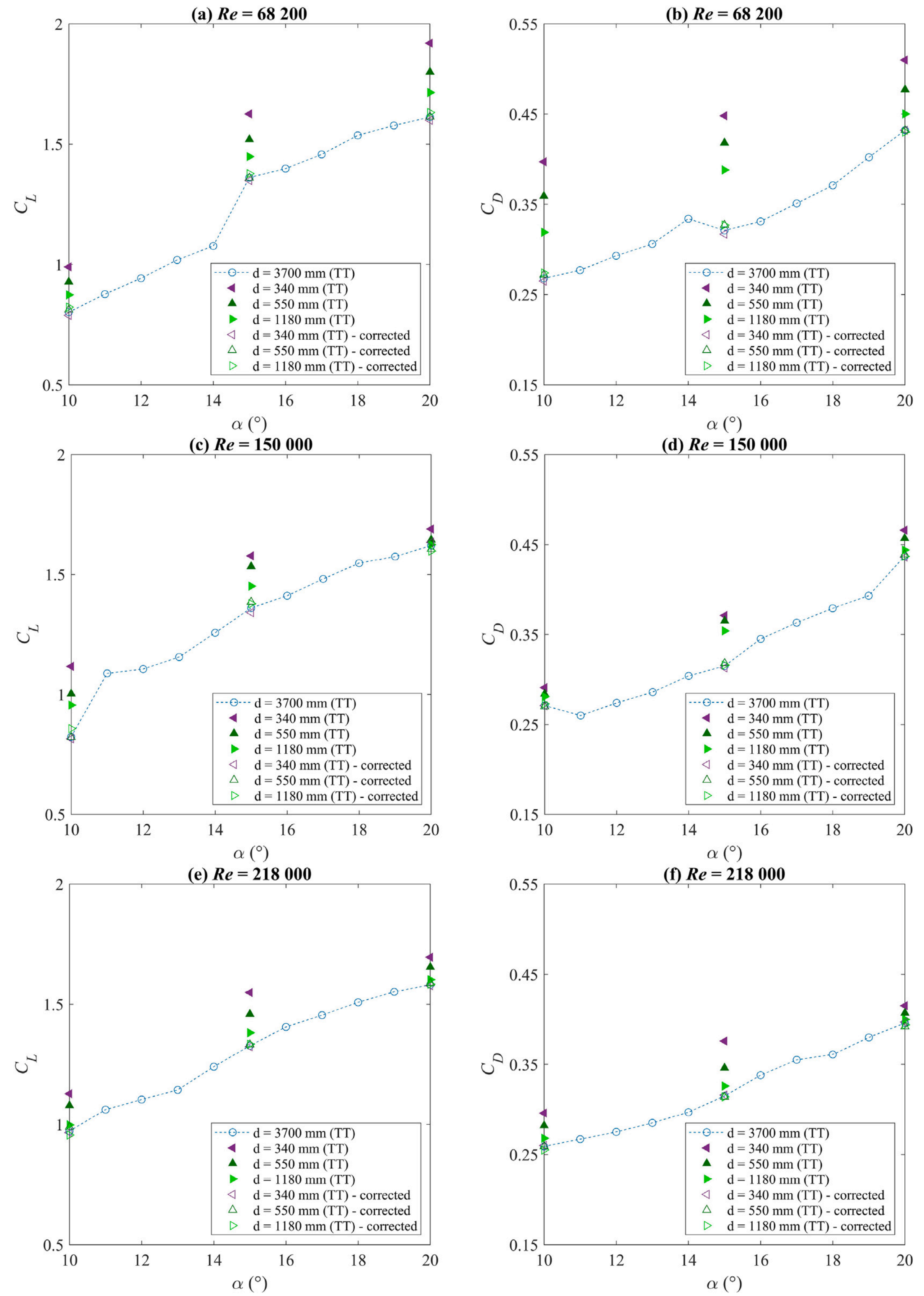

Fig. 9. Measured and corrected lift (a) and drag (b) coefficients versus the angle of attack for the various towing tank blockage ratios at Re = 68 200 (a–b), Re = 150 000 (c–d), and Re = 218 000 (e–f).

respectively. Note that experiments at Re = 150 000 and Re = 218 000 could not be performed in the water tunnel because the hydrodynamic moment would have exceeded the maximum range of the load cells.

The corrected drag is on average within 1.1% of the unblocked values. The corrected lift coefficient is on average within 1.87% of the unblocked data for $10° \leq \alpha \leq 17°$. This increases to 3.99% for $\alpha > 17°$. The divergence in the lift coefficient for high incidences ($\alpha > 17°$) is not to be attributed to an ineffective blockage correction. The discrepancy, which occurs for $A_F/A_S \geq 0.2288$, is due to the free surface deformation, and it is absent when a top plate is employed.

In contrast, for both the lift and the drag coefficients, neither of the two ESDU blockage corrections (ESDU, 1995, 1998) collapse on the unblocked result. The ESDU 76028 includes both a correction to the dynamic pressure due to the solid-body and wake blockage, resulting in a vertical shift of each data point in Fig. 10, and a correction to the angle of attack, resulting in a horizontal shift of each data point. The blocked and the unblocked measurements show the force crisis for $14^\circ < \alpha < 15^\circ$, and thus a correction of the angle of attack should be null or smaller than 1°. Indeed, Eq. (14) results in a correction of the order of 0.1°. Hence, the magnitude of the angle of attack correction is consistent with the present results.

The corrections to the dynamic pressure computed with ESDU 76028 (Eq. (12)) and ESDU 80024 (Eq. (15)) are similar: they converge for vanishing α and the ESDU 76028 correction is less severe than that computed with ESDU 80024. Both corrections increase with α and result in a better prediction of the unblocked force (d = 3700 mm (TT) in Fig. 10) at $\alpha \approx 20$ than at lower α. However, both corrections are insufficient and the corrected forces do not collapse on the unblocked forces. It is noted that only a negligible improvement is achieved if the arc is considered as full, i.e. solving Eq. (12) and (15) assuming $t = y_c$.

The most severe correction between the two ESDU guidelines is achieved with Eq. (15) for ESDU 80024. C_F/C_{FB} ranges from 0.94 at $\alpha = 10^\circ$ and 0.86 at $\alpha = 20^\circ$, i.e. it decreases with α. In contrast, a good fit of the data would be achieved with a correction that had the opposite trend. Such a trend cannot be achieved with Eq. (15) for any physical value of the input parameters. In fact, both the blockage ratio H_F/d and the blocked drag coefficient C_DB increase monotonically with α (but for the critical angle of attack where C_{DB} decreases), and thus C_F/C_{FB} decreases monotonically with α.

The disagreement is possibly due to two separate effects. Firstly, the ESDU corrections considered in this work do not take into account of the two separate flow regimes, subcritical and supercritical. Secondly, the volume of the wake, or its effect on the dynamic pressure, seems substantially underestimated. At the subcritical angles of attack ($\alpha \leq 14^\circ$), the volume of the wake associated with laminar separation is probably much greater than estimated by the guidelines, which assume a turbulent flow regime. A correction C_F/C_{FB} as low as ca. 0.7 would be necessary to ensure a good fit with our experiments, instead of ca. 0.9 as predicted by ESDU 80024. The choice of the ESDU correction is based on the Reynolds number and the blocked drag coefficient, whose values point at a correction for turbulent flow. Indeed, also in the case of the circular arc, the boundary layer turns to turbulent near the leading edge, but the boundary layer laminarises because of the flow acceleration (Souppez et al., 2022). However, also the ESDU formulations for low Reynolds number flow would underestimate the required correction. For example, ESDU 80024, Section 4.1, gives $C_F/C_{FB} = 1 - mH_F/d$, where the maximum value of m is 2.06 for an equilateral wedge with a side normal to the flow. This formulation gives a correction of about 0.8 at $\alpha = 10^\circ$.

Also at supercritical angles of attack ($\alpha \leq 14^\circ$), the volume of the wake is likely to be underestimated by the ESDU guidelines. In fact, the predicted correction is about 0.9, while 0.8 would result in a better agreement with our experiments. This suggests that the volume of the wake of the circular arc is consistently underestimated by current guidelines. This could possibly be due to the hybrid nature of the arc, which is neither a streamlined nor a bluff body. The ESDU 76028 correction assumes a foil with marginal flow separation, resulting in a thin wake leaving the foil with a direction parallel to the trailing edge. Conversely, the massive trailing edge separation of the circular arc results in a bluff-body-type separation and a much thicker wake. The ESDU 80024 assumes a bluff-body-type separation, with a wake thickness comparable to the frontal height H_F of the body. However, the flow on the pressure side of the arc (i.e. the concave side) leaves the arc with a direction parallel to the trailing edge, as for a streamlined foil where the Kutta condition is established. Therefore, the shear layer is projected outwards increasing the thickness of the wake. This hybrid nature of the circular arc, such that the leading-edge shear layer behaves like a bluff body, while the trailing-edge shear layer behaves like a streamlined body, might be the reason for the underestimated wake volume by the ESDU guidelines.

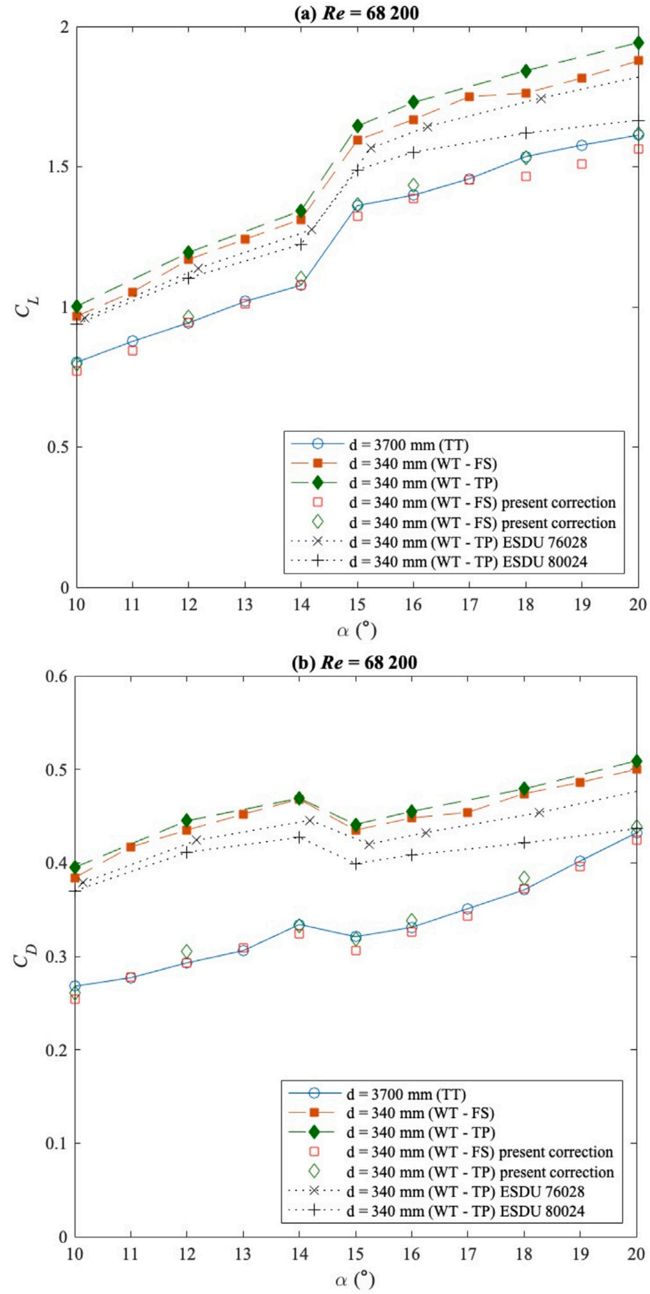

Fig. 10. Measured and corrected lift (a) and drag (b) coefficients versus the angle of attack at Re = 68 200 for tests undertaken with a top plate (TP) and free surface (FS), and corrections from ESDU 76028 and ESDU 80024 guidelines.

4. Conclusions

Force measurements on two-dimensional circular arcs with a camber-to-chord ratio of 0.2232 were undertaken over a range of blockage ratios from 0 to 0.2477 through experiments in a water tunnel and a towing tank. Tests were performed at positive incidences between the ideal angle of attack and deep-stall, over a transitional Reynolds number range between Re = 53 530 and Re = 218 000. The thickness-to-chord ratio of the models was smaller than 0.018 and its effect was found to be negligible. Thus, the results can be generalised to infinitely thin curved plates.

It was found that both the lift and the drag increase linearly with the blockage ratio for any tested condition. Hence, for this geometry, it is possible to predict the unblocked lift and drag even when the blockage ratio is higher than recommended by conventional guidelines. This is particularly relevant to experiments where larger models are employed to achieve a better spatial resolution for flow visualisation.

The force crisis is unaffected by the blockage ratio, within the 1° increment employed in this study. Specifically, transition from subcritical to supercritical occurs at the same critical angle of attack and Reynolds number as for the unblocked condition. This result is important to inform the minimum scale of models representing arcs operating at a high Reynolds number.

A comparison with the blockage corrections ESDU 76028 and ESDU 80024 for streamlined and bluff bodies, respectively, showed that the proposed solid-body and wake blockage correction is significantly more severe than current guidelines.

The limit of usability of the proposed corrections could not be explored in this study. However, it was found unreliable for blockage ratios of 0.2288 and above, when tests were performed in a water tunnel without a top plate (and thus allowing free surface deformation), at a Reynolds number of 68 200 and a Froude number of 0.19.

These findings provide new insights into high blockage corrections for lifting foils with massive flow separation at transitional Reynolds numbers, and applications such as turbo-compressors, micro aerial vehicles, yacht sails and hydrofoils. They may allow refinement of experimental procedures for accurate accounting of blockage effects, may extend the range of model sizes that can be tested in water and wind tunnels and may contribute to the development of future guidelines for blockage corrections.

CRediT authorship contribution statement

Jean-Baptiste R.G. Souppez: Methodology, Validation, Formal analysis, Investigation, Writing – original draft. **Ignazio Maria Viola:** Conceptualization, Writing – review & editing, Supervision.

Declaration of competing interest

The authors declare that they have no known competing financial interests or personal relationships that could have appeared to influence the work reported in this paper.

Data availability

Data will be made available on request.

Acknowledgments

This work received funds from the School of Maritime Science and Engineering of Solent University, the Maritime Trust Fund via the 2018 Research, Knowledge Exchange, and Innovation Award, and the Institute of Marine Engineering, Science, and Technology via the 2019 Stanley Grey Fellowship.

References

Alexander, A., 1978. Wind Tunnel Corrections for Savonius Rotors. Vol. 1. NASA STI/Recon Technical Report A, pp. E6_69–E6_80.

Allen, J.H., Vincenti, W.G., 1944. Wall Interference in a Two-Dimensional-Flow Wind Tunnel with Consideration of the Effect of Compressibility. Technical Report, National Advisory Committee for Aeronautics, Report 4K03.

Arredondo-Galeana, A., 2019. A Study of the Vortex Flows of Downwind Sails (Ph.D. thesis). Insitute for Energy Systems, University of Edinburgh.

Barlow, J.B., Rae, W.H., Pope, A., 1999. Low-Speed Wind Tunnel Testing, third ed. John Wiley & Sons, New York.

Bot, P., 2020. Force variations related to flow pattern changes around a high-camber thin wing. AIAA J. 58 (5), 1906–1912. http://dx.doi.org/10.2514/1.J058443.

Bot, P., Rabaud, M., Thomas, G., Lombardi, A., Lebret, C., 2016. Sharp transition in the lift force of a fluid flowing past nonsymmetrical obstacles: evidence for a lift crisis in the drag crisis regime. Phys. Rev. Lett. 117 (23), 234501. http://dx.doi.org/10.1103/PhysRevLett.117.234501.

Collie, S., Jackson, P., Gerritsen, M., Fallow, J., 2004. Two-dimensional CFD-based parametric analysis of downwind sail designs. Int. J. Small Craft Technol. 146 (B1), http://dx.doi.org/10.3940/rina.ijsct.2004.b1.19041.

Coutanceau, M., Bouard, R., 1977. Experimental determination of the main features of the viscous flow in the wake of a circular cylinder in uniform translation. Part 1. Steady flow. J. Fluid Mech. 79 (2), 231–256. http://dx.doi.org/10.1017/S0022112077000135.

Cowdrey, C., 1968. Application of Maskell's theory of wind-tunnel blockage to some large solid models. In: Proc. Symp. of Wind Effects on Buildings and Structures, Loughborough University, UK. p. 29.

Cyr, S., Newman, B., 1996. Flow past two-dimensional membrane aerofoils with rear separation. J. Wind Eng. Ind. Aerodyn. 63 (1–3), 1–16. http://dx.doi.org/10.1016/S0167-6105(96)00065-7.

Dalton, C., 1971. Allen and vincenti blockage corrections in a wind tunnel. Aiaa J. 9 (9), 1864–1865. http://dx.doi.org/10.2514/3.6435.

Damak, A., Driss, Z., Abid, M., 2018. Optimization of the helical savonius rotor through wind tunnel experiments. J. Wind Eng. Ind. Aerodyn. 174, 80–93. http://dx.doi.org/10.1016/j.jweia.2017.12.022.

Dewavrin, J., Souppez, J.-B.R., 2018. Experimental investigation into modern hydrofoil-assisted monohulls: How hydrodynamically efficient are they? Trans. R. Inst. Nav. Archit. B Int. J. Small Craft Technol. 160 (B2), 111–120.

ESDU, 1995. Lift-Interference and Blackage Corrections for Two-Dimensional Subsonic Flow in Ventilated and Closed Wind-Tunnels. Technical Report, ESDU 76028, The Royal Aeronautical Society.

ESDU, 1998. Blockage Corrections for Bluff Bodies in Confined Flows. Technical Report, ESDU 80024, The Royal Aeronautical Society.

Glauert, H., 1933. Wind Tunnel Interference on Wings, Bodies and Airscrews. Technical Report, Aeronautical Research Council R&M No 1566, London (UK).

Hackett, J., Cooper, K., 2001. Extensions to Maskell's theory for blockage effects on bluff bodies in a closed wind tunnel. Aeronaut. J. 105 (1050), 409–418. http://dx.doi.org/10.1017/S0001924000012380.

Hein, B.R., Chopra, I., 2007. Hover performance of a micro air vehicle: rotors at low Reynolds number. J. Am. Helicopter Soc. 52 (3), 254–262. http://dx.doi.org/10.4050/JAHS.52.254.

ISO, 1998. Coated Abrasives—Grain Size Analysis—Part 1: Grain Size Distribution Test. Technical Report, International Organization for Standardization.

ITTC, 2011. ITTC recommended procedures - fresh water and seawater properties. In: International Towing Tank Conference.

ITTC, 2014. ITTC recommended procedures and guidelines: General guideline for uncertainty analysis in resistance test. In: ITTC Recommended Procedures and Guidelines, Procedure.

ITTC, 2017. ITTC quality system manual - recommended procedures and guidelines - procedure - ship models. In: International Towing Tank Conference.

Jeong, H., Lee, S., Kwon, S.-D., 2018. Blockage corrections for wind tunnel tests conducted on a darrieus wind turbine. J. Wind Eng. Ind. Aerodyn. 179, 229–239. http://dx.doi.org/10.1016/j.jweia.2018.06.002.

Kellnerová, R., Kukačka, L., Jurčáková, K., Uruba, V., Jaňour, Z., 2012. PIV measurement of turbulent flow within a street canyon: detection of coherent motion. J. Wind Eng. Ind. Aerodyn. 104, 302–313. http://dx.doi.org/10.1016/j.jweia.2012.02.017.

Lasher, W.C., 2001. Computation of two-dimensional blocked flow normal to a flat plate. J. Wind Eng. Ind. Aerodyn. 89 (6), 493–513. http://dx.doi.org/10.1016/S0167-6105(00)00076-3.

Lasher, W.C., Sonnenmeier, J.R., 2008. An analysis of practical RANS simulations for spinnaker aerodynamics. J. Wind Eng. Ind. Aerodyn. 96 (2), 143–165. http://dx.doi.org/10.1016/j.jweia.2007.04.001.

Lasher, W.C., Sonnenmeier, J.R., Forsman, D.R., Tomcho, J., 2005. The aerodynamics of symmetric spinnakers. J. Wind Eng. Ind. Aerodyn. 93 (4), 311–337. http://dx.doi.org/10.1016/j.jweia.2005.02.001.

Lieblein, S., 1960. Incidence and deviation-angle correlations for compressor cascades. J. Basic Eng. 82 (02), 575–584. http://dx.doi.org/10.1115/1.3662666.

Malizia, F., Blocken, B., 2020. Bicycle aerodynamics: History, state-of-the-art and future perspectives. J. Wind Eng. Ind. Aerodyn. 200, 104134. http://dx.doi.org/10.1016/j.jweia.2020.104134.

Marchand, J.-B., Astolfi, J.A., Bot, P., 2017. Discontinuity of lift on a hydrofoil in reversed flow for tidal turbine application. Eur. J. Mech. B Fluids 63, 90–99. http://dx.doi.org/10.1016/j.euromechflu.2017.01.016.

Maskell, E., 1963. A Theory of the Blockage Effects on Bluff Bodies and Stalled Wings in a Closed Wind Tunnel. Technical Report, Aeronautical Research Council, R&M no 3400, London (UK).

Miklasz, K., LaBarbera, M., Chen, X., Socha, J., 2010. Effects of body cross-sectional shape on flying snake aerodynamics. Exp. Mech. 50 (9), 1335–1348. http://dx.doi.org/10.1007/s11340-010-9351-5.

Molina, A.C., De Troyer, T., Massai, T., Vergaerde, A., Runacres, M.C., Bartoli, G., 2019. Effect of turbulence on the performance of VAWTs: An experimental study in two different wind tunnels. J. Wind Eng. Ind. Aerodyn. 193, 103969. http://dx.doi.org/10.1016/j.jweia.2019.103969.

Pankhurst, R.C., Holder, D.W., 1952. Wind-Tunnel Technique: An Account of Experimental Methods in Low-and High-Speed Wind Tunnels. Pitman.

Pope, A., Harper, J., 1966. Low-Speed Wind Tunnel Testing. Wiley, New York.

Prasanth, T., Behara, S., Singh, S., Kumar, R., Mittal, S., 2006. Effect of blockage on vortex-induced vibrations at low Reynolds numbers. J. Fluids Struct. 22 (6–7), 865–876. http://dx.doi.org/10.1016/j.jfluidstructs.2006.04.011.

Ross, I., Altman, A., 2011. Wind tunnel blockage corrections: Review and application to savonius vertical-axis wind turbines. J. Wind Eng. Ind. Aerodyn. 99 (5), 523–538. http://dx.doi.org/10.1016/j.jweia.2011.02.002.

Schewe, G., 2001. Reynolds-number effects in flow around more-or-less bluff bodies. J. Wind Eng. Ind. Aerodyn. 89 (14–15), 1267–1289. http://dx.doi.org/10.1016/S0167-6105(01)00158-1.

Schmitz, F., 1942. Aerodynamik des Flugmodells Traflügelmessungen: CJE Volckmann Nache E. E. Wette, Berlin-Charlottenburg.

Souppez, J.-B.R.G., Bot, P., Viola, I.M., 2021. On the effect of the leading-edge separation bubble on the aerodynamics of spinnakers. In: 7th High Performance Yacht Design (HPYD7), Auckland, New Zealand.

Souppez, J.-B.R.G., Bot, P., Viola, I.M., 2022. Turbulent flow around circular arcs. Phys. Fluids 34 (1), 015121. http://dx.doi.org/10.1063/5.0075875.

Souppez, J.-B.R.G., Viola, I.M., 2022. Development of a blockage correction for highly cambered 2D circular arcs. In: 24th Chesapeake Sailing Yacht Symposium. Society of Naval Architects and Marine Engineers, http://dx.doi.org/10.5957/CSYS-2022-003.

Tank, J.D., Klose, B.F., Jacobs, G.B., Spedding, G.R., 2021. Flow transitions on a cambered airfoil at moderate Reynolds number. Phys. Fluids 33 (9), 093105. http://dx.doi.org/10.1063/5.0061939.

Toebes, G., 1971. The frequency of oscillatory forces acting on bluff cylinders in constricted passages. In: Proc. of 14th Congress of International Hydraulic Research, Paris, France, Vol. 2. p. 58.

Velychko, N., 2014. Study of Highly Cambered Aero Foil Using JR3 Sensor. The University of Auckland, Department of Mechanical Engineering.